Energy Conversion and Management 113 (2016) 312–320

Contents lists available at ScienceDirect

Energy Conversion and Management

journal homepage: www.elsevier.com/locate/enconman

Variations of the bacterial foraging algorithm for the extraction of PV module parameters from nameplate data

Mohamed A. Awadallah [1]

Centre for Urban Energy, Ryerson University, 350 Victoria Street, Toronto, ON M5K 2B3, Canada

ARTICLE INFO

Article history:
Received 20 November 2015
Accepted 29 January 2016
Available online 10 February 2016

Keywords:
Bacterial foraging
Optimization
Parameter extraction
PV modules

ABSTRACT

The paper introduces the task of parameter extraction of photovoltaic (PV) modules as a nonlinear optimization problem. The concerned parameters are the series resistance, shunt resistance, diode ideality factor, and diode reverse saturation current for both the single- and double-diode models. An error function representing the mismatch between computed and targeted performance is minimized using different versions of the bacterial foraging (BF) algorithm of global search and heuristic optimization. The targeted performance is obtained from the nameplate data of the PV module. Five distinct variations of the BF algorithm are used to solve the problem independently for the single- and double-diode models. The best optimization results are obtained when swarming is eliminated, chemotactic step size is dynamically varied, and global best is preserved, all acting together. Under such conditions, the best global minimum of 0.0028 is reached in an average best time of 94.4 sec for the single-diode model. However, it takes an average of 153 sec to reach the best global minimum of 0.0021 in case of double-diode model.

An experimental verification study involves the comparison of computed performance to measurements on an Eclipsall PV module. It is shown that all variants of the BF algorithm could reach equivalent-circuit parameters with accepted accuracy by solving the optimization problem. The good matching between analytical and experimental results indicates the effectiveness of the proposed method and validates research findings.

1. Introduction

In response to the global warming issue and depletion of classical fossil fuels, increasing attention has been recently directed toward renewable energy sources. Solar energy seems to be a promising choice of clean and inexhaustible sources. Solar energy comes next to wind as the fastest developing renewable energy source. Radiant light and heat of the sun are harnessed via a variety of ever-evolving technologies. Photovoltaic (PV) cells convert the energy of sun light into DC electricity, which is usually inverted into AC before being transmitted through power networks or consumed by local loads.

The output characteristics of a PV cell are highly nonlinear, so are the effects of equivalent-circuit parameters on computed performance. Therefore, the accurate estimation of parameters is imperative to the modeling, simulation, analysis, and control of PV modules. Most of the parameter extraction techniques available in the literature depend on analytical manipulations of the mathematical model equations to express the parameters in terms of output variables [1–11]. Information about module performance is required to calculate the parameters; such information is obtained either from manufacturer datasheet [1–6] or from experimental measurements [5–11]. However, the mathematical expressions of the parameters in terms of the output variables are complicated and require numerical iterative methods for solution [3–9]. Direct solution of such equations is also possible in case some approximating assumptions are followed [1,2,10], and [11].

Curve fitting is employed to fit computed performance to experimental measurements with minimal error for parameter extraction purposes [11–14]. A variety of curve fitting techniques is implemented including least-square method over the whole operating region [12], voltage fitting near open circuit and current fitting near short circuit [13], and auxiliary function fitting [14].

Nature-inspired algorithms for global search and heuristic optimization – such as genetic algorithms (GA), differential evolution (DE), particle swarm optimization (PSO), bacterial foraging (BF), simulated annealing (SA), and artificial immune systems (AIS) – are also applied to PV parameter extraction [15–21]. The benchmark performance of the parameter extraction process is obtained either from manufacturer datasheet [15–17], or from experimentation [18–21]. In [15,16], the objective function

[1] On leave from University of Zagazig, Egypt.
E-mail address: awadalla@ryerson.ca

http://dx.doi.org/10.1016/j.enconman.2016.01.071
0196-8904/

represents the rate of change of module current with respect to voltage at the maximum power point (MPP). Whereas, the discrepancy between measured and computed current signifies an objective function to be minimized in [18–20]. In [21], simulated annealing is used to extract the parameters of single- and double-diode PV models from measured module performance.

The PV model parameters may slightly change with loading or with the variation of environmental conditions. A statistical analysis based on Monte Carlo simulations is employed to evaluate the uncertainty in the estimation of the series and shunt resistances in the double-diode PV model [22]. Nevertheless, for accurate simulation, the parameters have to be precisely identified. The precision of PV parameters plays a critical role in estimating the panel performance through irradiance and temperature dependent models [23].

Inspired by the foraging theory of *Escherichia coli* bacteria, Passino [24] proposed the bacterial foraging (BF) algorithm for distributed optimization in 2002. The algorithm found immediate engineering applications including, but not limited to, optimal power flow [25], control design of electrical drives [26], unit commitment [27], optimal feeder routing [28], automatic generation control [29], distribution network balancing [30], harmonic estimation [31], load compensation [32], and optimum economic dispatch [33]. However, the BF algorithm is claimed to have poor convergence characteristics on high dimensional problems.

Many researchers proposed various enhancements on the mechanism of BF algorithm, especially the run size taken by a bacterium during chemotaxis. An adaptive run size, which dynamically decreases as the chemotactic steps progress, is suggested in [33]. A user-defined parameter of the BF algorithm is also used to adapt the run size [34]. In [35], a self-adaptive step size is based on the objective function value of the bacterium and whether or not the global minimum is zero. Another self-adaptation procedure is proposed in [36], where a bacterium changes its run length to switch between exploration of the search space and exploitation of a potential subspace. It is claimed in [37] that when a selection process replaces the reproduction and elimination-dispersal steps together, the BF algorithm becomes more suited to dynamic environments. The selection probability of a bacterium depends on its fitness and rank among the population. In [38], reproduction is completed through crossover. A certain number of least healthy bacteria die, while an equal number of healthiest bacteria undergo crossover to yield the same number of offspring. A list of improving modifications to the BF algorithm is reported in [39]. The nested-loop structure of the algorithm is avoided, and the limited swim runs are opened such that a bacterium swims as long as it finds more nutrient. The run length per bacterium is adapted based on the improvement of the objective function. A new chemotactic strategy is suggested such that a bacterium moves only if it finds a lesser value of the objective function [39]. Another approach of improving the convergence behavior of the BF algorithm is via hybridization with other heuristic optimization routines such as GA [40], DE [41], and PSO [42].

This paper presents an optimization-based technique for the extraction of PV module parameters from nameplate data. The mismatch between computed and targeted performance is minimized. Targeted performance includes the open-circuit voltage (V_{oc}), short-circuit current (I_{sc}), maximum power (P_{max}), and voltage at maximum power (V_{mp}), all under standard test conditions (STC) as attained from nameplate data of the module. The nonlinear optimization problem is solved for both single- and double-diode PV models using five variants of the BF algorithm. The algorithm variants include the original routine proposed in [24] and four modified versions. The first modification neglects the swarming effect of bacteria, whereas the run size is dynamically decreased using a linear function in the second modification. Since no inherent procedure immunes the algorithm against losing the global best objective function value, a third modification preserves the global best by preventing the corresponding bacterium from missing its current position by any foraging activity. Finally, a fourth variation of the BF algorithm aggregates all three previous modifications together. In the experimental verification study, the performance of the PV module is measured under different operating conditions and compared to computations using the best set of parameters for single- and double-diode models.

2. Mathematical modeling and problem statement

The single-diode model of a PV cell comprises a current source in parallel to a diode, a shunt resistor to account for leakage current, and a series resistor to represent losses related to load current, Fig. 1(a). Thus, the cell current is given by [3]

$$I_c = I_{ph} - I_{os}\left[e^{\frac{q}{AKT}(V_c+R_sI_c)} - 1\right] - \frac{(V_c + R_sI_c)}{R_{sh}} \tag{1}$$

where I_c is the cell current, Amps, I_{ph} is the photocurrent, Amps, I_{os} is the reverse saturation current of the diode, Amps, q is the electron charge, C, A is the diode ideality factor, K is Boltzmann constant, J/oK, T is the cell temperature, oK, V_c is the cell voltage, V, R_s is the series resistance, Ohm, and R_{sh} is the shunt resistance, Ohm. On the other hand, the photocurrent depends on the solar irradiance and cell temperature, and is expressed as [3]

$$I_{ph} = \lambda[I_n + k_i(T - T_r)] \tag{2}$$

where λ is the normalized solar irradiance, suns, I_n is the nominal short-circuit current at STC (1000 W/m^2 irradiance, 25 °C temperature, and 1.5 air mass), Amps, k_i is the short-circuit current temperature coefficient, Amps/°K, and T_r is the reference temperature, °K. Meanwhile, the reverse saturation current of the diode varies with temperature, and is given as [3]

$$I_{os} = I_{or}\left[\frac{T}{T_r}\right]^3 e^{\frac{qE_g}{AK}\left(\frac{1}{T_r}-\frac{1}{T}\right)} \tag{3}$$

where I_{or} is the reverse saturation current of the diode at reference temperature and irradiance, Amps, E_g is the band gap energy of the cell material, J/C. When PV cells are connected in series or parallel in order to raise the level of output voltage and current, Fig. 1(b), the output current is expressed as

$$I = N_pI_{ph} - N_pI_{os}\left[e^{\frac{q}{AKT}\left(\frac{V}{N_s}+\frac{R_sI}{N_p}\right)} - 1\right] - \frac{1}{R_{sh}}\left[\frac{N_p}{N_s}V + R_sI\right] \tag{4}$$

where N_p and N_s are the number of cells in parallel and series, respectively.

The performance of a PV cell is described by (1)–(3). The model correlates the output variables of the cell, V_c and I_c, with the independent variables set by environmental conditions, λ and T, through physical constants and system parameters. The Boltzmann constant (K), electron charge (q), band gap energy of the cell material (E_g), and reference temperature (T_r) are all constants. Whereas, series resistance (R_s), shunt resistance (R_{sh}), diode ideality factor (A), nominal short-circuit current (I_n), reverse saturation current at reference temperature and irradiance (I_{or}), and short-circuit current temperature coefficient (k_i) are parameters of the PV cell. Numbers of series and parallel cells are also required to compute the performance of a PV module using (4).

As shown in Fig. 2, in the double-diode model of a PV cell, two diodes are in parallel with the photocurrent source. The model is known to be more accurate than the single-diode model, especially at low irradiance levels. One diode represents the diffusion current

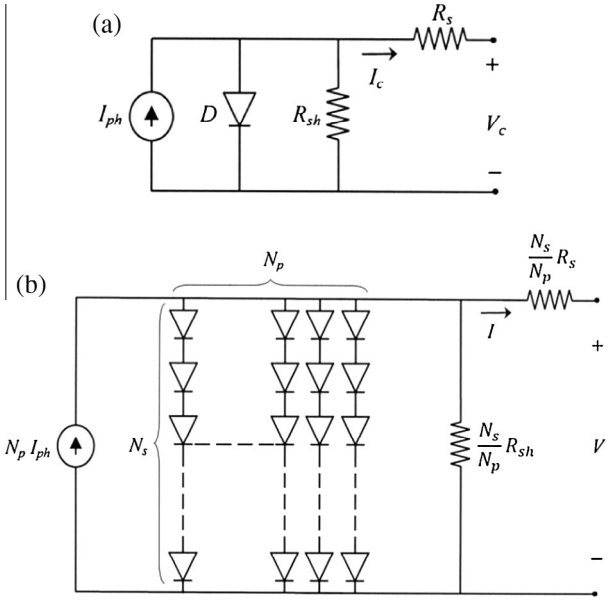

Fig. 1. Single-diode model of: (a) PV cell, and (b) PV array.

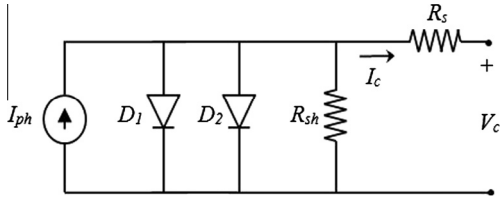

Fig. 2. Double-diode model of a PV cell.

in the *p*–*n* junction, whereas the other takes the space-charge recombination effect into account [43]. Both single- and double-diode models are widely accepted to represent the behavior of crystalline semiconductor PV cells. The output *I*–*V* characteristic equation of the double-diode model becomes

$$I_c = I_{ph} - I_{os1}\left[e^{\frac{q}{A_1 KT}(V_c+R_sI_c)} - 1\right] - I_{os2}\left[e^{\frac{q}{A_2 KT}(V_c+R_sI_c)} - 1\right] - \frac{(V_c+R_sI_c)}{R_{sh}} \tag{5}$$

The reverse saturation currents of the two diodes are expressed in terms of their values at reference temperature and irradiance as

$$I_{os1} = I_{or1}\left[\frac{T}{T_r}\right]^3 e^{\frac{qE_g}{A_1 K}\left(\frac{1}{T_r}-\frac{1}{T}\right)} \tag{6}$$

and

$$I_{os2} = I_{or2}\left[\frac{T}{T_r}\right]^3 e^{\frac{qE_g}{A_2 K}\left(\frac{1}{T_r}-\frac{1}{T}\right)} \tag{7}$$

Eqs. (5), (2), (6), and (7) represent the mathematical model based on the double-diode equivalent circuit. The model parameters are series resistance (R_s), shunt resistance (R_{sh}), ideality factors for both diodes (A_1 and A_2), nominal short-circuit current (I_n), reverse saturation current at reference temperature and irradiance for both diodes (I_{or1} and I_{or2}), and short-circuit current temperature coefficient (k_i). It is obvious that the second diode adds two parameters to the model. It should be mentioned that the nameplate of the PV module indicates the short-circuit current under STC, which is the nominal short-circuit current (I_n).

The objective of this research is to estimate the model parameters of PV modules by minimizing the discrepancy between computed and targeted performance. In other words, a set of parameters, which yields computed performance as close as possible to targeted performance, is sought. The targeted performance is attained from the nameplate data of the PV module. In the present work, targeted performance signifies four indices, i.e., V_{oc}, I_{sc}, P_{max}, and V_{mp} at STC as given in the module nameplate. Therefore, an acceptable set of parameters has to minimize the objective function that measures the discrepancy between computed and targeted performance. The present optimization problem is formulated as

$$\min_x J = \sum_{i=1}^{n} \frac{|X_{Ci} - X_{Ti}|}{X_{Ti}} \tag{8}$$

where x is the set of PV parameters, J is the objective function value, X_{Ci} is the ith computed performance index, X_{Ti} is the ith targeted performance index, and n is the number of performance indices. The problem is independently solved for the single- and double-diode models by five variants of the BF algorithm. The technique is applied to an Eclipsall NRG72 module, whose nameplate is shown in Fig. 3.

3. The bacterial foraging algorithm and Its variations

The BF optimization algorithm is based on the foraging theory of the *E. coli* bacteria which comprises three main activities, namely, chemotaxis, reproduction, and elimination-dispersal. Chemotaxis indicates the motion pattern of bacteria in the presence of chemical attractants and repellants. During a chemotactic step, a bacterium can either swim or tumble, where swimming means continuous movement in certain direction and tumbling indicates random change of direction. Asexual reproduction of the *E. coli* bacteria happens under certain conditions when a bacterium elongates then splits from the middle into two identical individuals. Elimination-dispersal probabilistically takes place due to sudden environmental changes. The bacteria may die affected by noxious substances, while new bacteria can be randomly generated at different location. While foraging, the *E. coli* bacteria have a tendency of swarming through communication by chemicals. The foraging theory is based on maximizing the energy gained per unit time. A bacterium is in continuous search of nutrient-rich media using its four-second memory to evaluate the nutrient gradient.

A computer program, which imitates foraging activities of the *E. coli* bacteria, can be used for optimizing a multi-modal nonlinear function with no derivative information required. In the optimization software, chemotaxis is modeled via a step taken by the bacterium in a random direction as

$$\theta^i(j+1,k,l) = \theta^i(j,k,l) + C(i)\frac{\Delta(i)}{\sqrt{\Delta^T(i)\cdot\Delta(i)}} \tag{9}$$

where $\theta^i(j+1,k,l)$ is the position of the ith bacterium at the $(j+1)$th chemotactic step, kth reproduction step, and lth elimination-dispersal event, $\theta^i(j,k,l)$ is the position of the ith bacterium at the jth chemotactic step, kth reproduction step, and lth elimination-dispersal event, $C(i)$ is the step length of the ith bacterium, and $\Delta(i)$ is a random vector in the search space. Therefore, swimming encompasses successive discrete runs with fixed step size as long as the objective function value improves. A maximum is set on the possible number of runs in a single swim to avoid trapping in local minima. The swarming effect is modeled by adding a value, representing the cell-to-cell communication, to the objective function. Such a value depends on the width and depth of the attractant and repellant chemicals released by one bacterium, and is given by

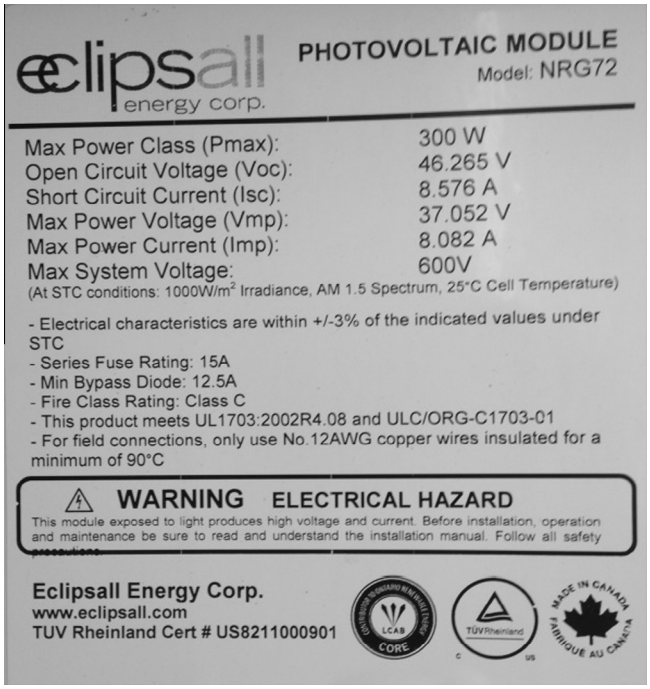

Fig. 3. Nameplate of the Eclipsall NRG72 PV module.

$$J_{cc}(\theta, P(j,k,l)) = \sum_{i=1}^{S}\left[-d_{attract}e^{\left(-w_{attract}\sum_{m=1}^{p}(\theta_m-\theta_m^i)^2\right)}\right] + \sum_{i=1}^{S}\left[h_{repell}e^{\left(-w_{repell}\sum_{m=1}^{p}(\theta_m-\theta_m^i)^2\right)}\right] \quad (10)$$

where $J_{cc}(\theta, P(j,k,l))$ is the cell-to-cell effect to be added to the objective function of the bacterium θ, $P(j,k,l)$ is the bacteria population at the jth chemotactic step, kth reproduction step, and lth elimination-dispersal event, S is the population size, $d_{attract}$ and $w_{attract}$ are the depth and width of attractant chemical, p is dimension of the search space, and h_{repell} and w_{repell} are the height and width of repellant chemical.

At each reproduction step, the bacteria population is ranked based on the associated values of objective function. Assuming the number of reproduced bacteria to be S_r, the worst S_r bacteria are deleted from the population, whereas the best S_r bacteria are split in half at the same position. Such a reproduction scenario assures fixed population size. The elimination-dispersal event takes place when N_{ed} bacteria are randomly eliminated from the population with a probability of p_{ed}, and an equal number of bacteria is dispersed at random positions of the search space. The flowchart of the BF optimization algorithm is shown in Fig. 4. The first BF version used in the present research represents the original algorithm as introduced in [24], and is denoted BF1.

3.1. Swarming

The social aspect of the biological foraging theory of the *E. coli* bacteria is transferred into the optimization algorithm through the cell-to-cell communication component in (10). Such a component is highly dependent on four user-defined parameters representing the width and depth of the attractant and repellant chemicals released by the bacteria. However, the component is added to the value of the objective function to be minimized. Although the chemical communication between bacteria assists the foraging activities in nature, the representing component in the optimization algorithm tends to obscure the actual value of the objective function. Close to the end of the optimization process, the objective function becomes highly sensitive to any added value, especially if the global minimum is zero. Accordingly, it is believed that ignoring the swarming effect in the bacteria population may have positive impact on the convergence behavior as well as the resulting solution. In the second version of the algorithm, denoted BF2, the cell-to-cell communication component given by (10) is disregarded.

3.2. Chemotactic step size

In natural foraging of the *E. coli* bacteria, the step size generally differs from one bacterium to another. Even for the same bacterium, the step size may vary from one swim to another, or may also vary from one run to another within the same swim. Nevertheless, in the original BF algorithm [24], the step size is considered constant for all bacteria throughout the optimization process.

The step size is characterized by many researchers as one vital parameter having serious influence on optimization dynamics and convergence behavior [33–36]. In addition, the step size has to satisfy some conditions in order to maintain the asymptotic stability of the search process [44]. The step size is preferred to have a high value at the beginning of the search process in order to promote exploration of the search space by different bacteria [36]. However, once a bacterium reaches a nutrient-rich neighborhood, its step size should reduce for better exploitation of the promising proximity [36]. In [39], the step size of a certain bacterium decreases by 20% if the corresponding objective function improves or stagnates, and increases by 20% otherwise. A good initial value of the step size is 1% of the main diagonal length of the search space [39].

A dynamically decreasing step size is adopted in the third variation of the BF algorithm, BF3. The step size monotonically decreases from an initial value, C_0, to a final value, C_f, as the optimization progresses. With regard to the nested-loop architecture of the algorithm, all bacterial steps in one chemotactic run are carried out with a fixed value of the step size. The step size is updated after the chemotactic loop is completed. The following chemotactic run has a reduced step size such that the step size decreases linearly between the two user-defined extremes, C_0 and C_f. Accordingly, the step size is updated right after the chemotactic loop by the following function

$$C(i,j+1) = C(i,j) - \frac{C_f - C_0}{N_{re}+N_{ed}-1} \quad (11)$$

where $C(i,j+1)$ is the step size of the ith bacterium during the $(j+1)$th chemotactic step, $C(i,j)$ is the step size of the ith bacterium during the jth chemotactic step, C_0 is the initial step size, C_f is the final step size, N_{re} is the number of reproduction steps, and N_{ed} is the number of elimination-dispersal events. Therefore, the bacteria move with a large step size at the beginning in order to explore the whole search space and discover its potential subspaces. The step size reduces linearly with time in order to allow the bacteria to better exploit the promising vicinities of the search space.

3.3. Preservation of global best function

The BF algorithm presented in [24] has no inherent procedure that preserves the global best value of the objective function. Literally, any bacterium can unrestrictedly undergo a chemotactic step, a reproduction step, or an elimination-dispersal event. Consequently, the position of the search space which yields the best value of the objective function is subject to being lost. The best

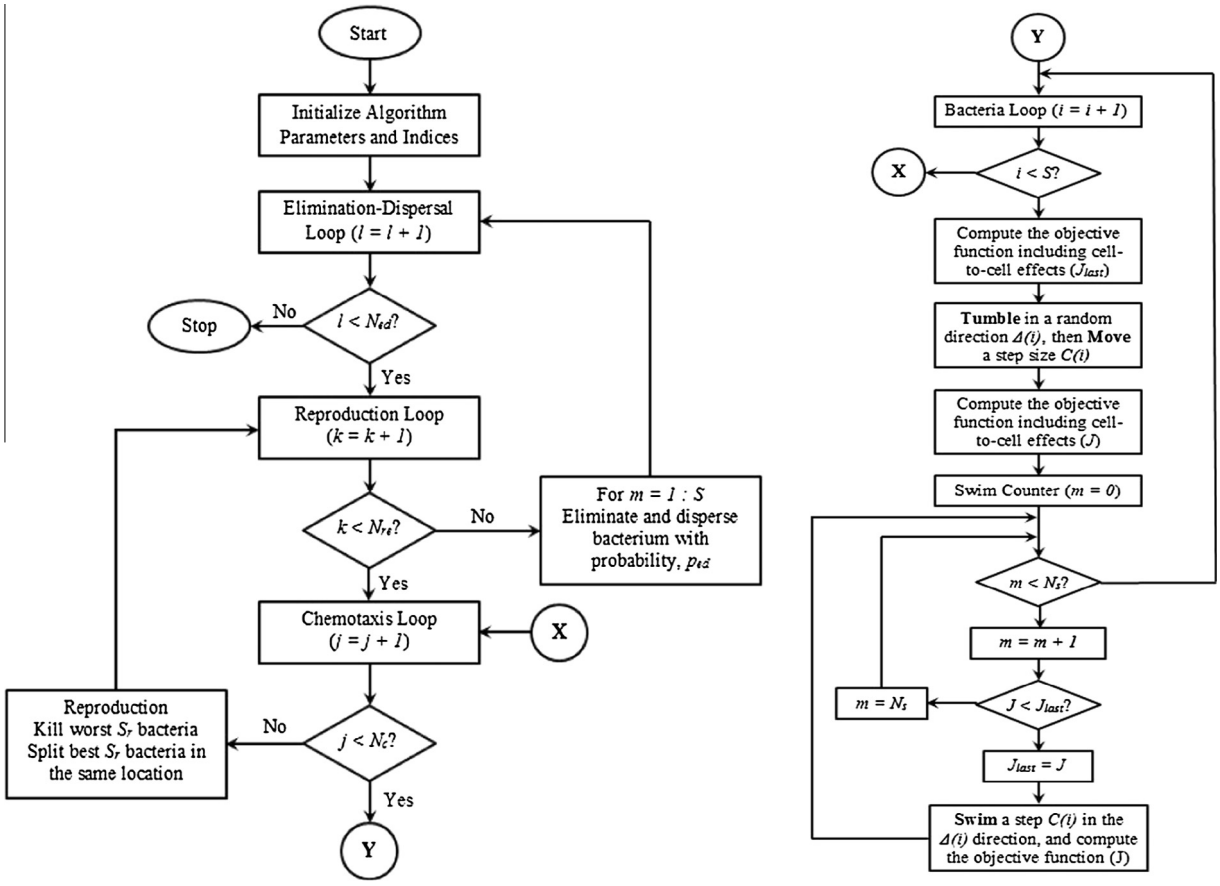

Fig. 4. Flowchart of the bacterial foraging algorithm.

objective function of the bacteria population at the last iteration is usually taken as solution of the optimization problem. Nothing assures that such solution gives the best value the population has ever come across.

In the fourth variant of the BF algorithm, denoted as BF4, the bacterium with the best global value of the objective function is identified. This bacterium is exempted from any foraging activity, i.e. chemotaxis, reproduction, and elimination-dispersal, in order for the population not to lose the global best function. The best bacterium is fixed in space until another bacterium is able to find a better value of the objective function in the following iterations, and so on. Therefore, the best objective function of the population either improves or stagnates.

The fifth, and last, version of the BF algorithm incorporates all three proposed modifications together. In other words, the fifth version, identified as BF5, ignores swarming, employs dynamic adaptive step size, and preserves the global best function value. So, the fifth variant combines all advantages of the proposed algorithm modifications, and is expected to yield best optimization results. Table 1 shows the different features of the BF algorithm variations used in the present work.

Table 1
Features of the BF algorithm variations.

Feature	BF1	BF2	BF3	BF4	BF5
Swarming	✓	×	✓	✓	×
Fixed step size	✓	✓	×	✓	×
Preservation of global best	×	×	×	✓	✓

4. Optimization results

The five variations of the BF algorithm described above are used to extract the parameters of the Eclipsall PV module from its nameplate data shown in Fig. 3. The algorithm versions which do not adopt swarming, i.e., BF2 and BF5, minimize the basic objective function, J, given in (8). However, versions which implement swarming, i.e., BF1, BF3, and BF4, minimize the overall objective function, $J + J_{cc}$, whose components are given in (8) and (10). The parameters of the BF algorithm used in solving the present problem are shown in Table 2. The five BF variations are run for 50 times each on both the single- and double-diode models. Optimization results over the 50 runs of each BF variation are shown in Table 3. It should be emphasized that multiple runs of the algorithms are deemed to reduce the impact of the inherent randomness on results.

Convergence behaviors of the runs which yield the best values of the basic objective function, J, are plotted in Figs. 5 and 6 for the single- and double-diode models, respectively. The PV model parameters corresponding to the minimum basic objective function, J, are given in Table 4. It should be clearly stated that the algorithm run which yields minimum basic objective function, J, does not necessarily yield minimum overall objective function, $J + J_{cc}$, in case swarming is implemented, i.e., in cases of BF1, BF3, and BF4.

On comparing the behaviors of different BF variations, reference will be always made to the original algorithm proposed in [24], BF1. This version of the algorithm applies swarming, runs with fixed step size, and does not preserve global best function. Impacts of such three features, either individually or collectively, on the optimization process are to be examined. Comparison between different variations will focus on the ability to minimize the basic

Table 2
Parameters of the BF Algorithm.

Basic parameters	
Dimension of search space, p	5 for single-diode model, and 7 for double-diode model
Number of bacteria, S	$10 \times p$
Number of chemotactic steps, N_c	50
Number of reproduction steps, N_{re}	5
Number of elimination-dispersal events, N_{ed}	2
Number of runs in a swim, N_s	5
Number of reproduced bacteria, S_r	$S/2$
Elimination-dispersal probability, p_{ed}	0.25
Chemotactic step size, C	$0.01 \times d$[a]
Swarming parameters	
Attractant depth, $d_{attract}$	0.001
Attractant width, $w_{attract}$	0.3
Repellant height, h_{repell}	0.001
Repellant width, w_{repell}	0.6
Adaptive step-size parameters	
Initial chemotactic step size, C_0	$0.03 \times d$[a]
Final chemotactic step size, C_f	$0.003 \times d$[a]

[a] d is the main diagonal length of search space.

objective function, J, even when swarming is adopted. The reason is that, according to the definition of the optimization problem in (8), the less the value of J, the better the obtained parameters represent the behavior of the PV module under consideration.

The algorithm version BF2 neglects swarming, i.e., BF2 minimizes the basic objective function, J, since the swarming component, J_{cc}, is not computed. When comparing BF2 to BF1 on the basis of the objective function seen by the algorithm, BF1 finds a minimum ($J + J_{cc}$) of 0.0015 and −0.009 on the single- and double-diode models, respectively. Whereas, BF2 attains a minimum J of 0.0082 and 0.0061 on single- and double-diode models respectively. Therefore, eliminating the swarming effect helps the BF algorithm realize a better objective function. However, a comparison based on the obtained basic objective function, J, is more realistic for the purpose of the present study. It is obvious that J is the objective function component which assesses the quality of the obtained parameters. Unfortunately, disregarding swarming component by itself does not help the BF algorithm obtain better parameter set for the PV module. On the other hand, the convergence time drastically improved due to the reduction of the computational burden per iteration from BF1 to BF2. The convergence curves of BF1 in Figs. 5 and 6 tend to be at lower values of those of BF2. The reason is that the swarming component, J_{cc}, is always negative according to the parameters given in Table 2.

Dynamically varying chemotactic steps are assumed in BF3 according to (11) and Table 2 parameters. Such a variation allows the algorithm to better explore the search space at the beginning of iteration, and to better exploit potential subspaces when iteration approaches its end. Comparing to BF1, BF3 does not improve either the overall function, $J + J_{cc}$, or the basic function, J, on any model as could be noticed from Table 3 results. The changes caused by the dynamic step size on convergence time, Table 3, and convergence behavior, Figs. 5 and 6, are inconclusive.

The algorithm version BF4 protects the global best function from being lost due to chemotaxis or elimination-dispersal. The first distinction from BF1 is noticed in Figs. 5 and 6. The objective function fluctuates on the convergence curves of BF1 since the values could decrease due to search progress or increase due to loss of global best. However, objective function on BF4 curves stagnates at the same value as a result of global best preservation or decreases if better value is found. Changes of convergence time from BF1 to BF4 are inconclusive as seen in Table 3. Most importantly, both basic and overall objective functions improve on both single- and double-diode models by the preservation of global best. The improvements of J from 0.0076 to 0.003 on single-diode model, and from 0.0045 to 0.0026 on double-diode model, are significant. Therefore, it could be stated that, out of the three suggested variations, preservation of global best is most effective in attaining a better solution of the present optimization problem leading to a more accurate parameter set of the PV module.

The last version, BF5, combines the suggested variations altogether. Thus, it is expected also to gather all the benefits, and yield best results. Due to preservation of global best, objective functions of BF5 do not fluctuate, Figs. 5 and 6. Due to elimination of swarming effect, convergence times are less than those of other algorithm

Table 3
Optimization results.

Algorithm			BF1	BF2	BF3	BF4	BF5
Single-diode model							
Convergence time, s		Min	172.46	90.76	154.42	166.06	89.7
		Mean	189.37	100.23	169.65	177.96	94.4
		Stdev	7.83	8.59	7.01	7.66	3.09
Objective function	Basic, J	Min	0.0076	0.0082	0.0079	0.003	**0.0028**
		Mean	0.0116	0.0112	0.0111	0.0058	0.0055
		Stdev	0.0019	0.0016	0.0016	0.0019	0.0015
	Swarming, J_{cc}	Min	−0.008	–	−0.007	−0.01	–
		Mean	−0.005	–	−0.005	−0.008	–
		Stdev	0.0012	–	0.0011	0.001	–
	Overall, $J + J_{cc}$	Min	0.0015	–	0.0019	−0.007	–
		Mean	0.0062	–	0.0064	−0.002	–
		Stdev	0.0025	–	0.0018	0.0022	–
Double-diode model							
Convergence time, s		Min	279.06	122.07	294.78	299.12	121.97
		Mean	308.79	144.45	315.52	313.57	153
		Stdev	12.7	4.87	15.76	13.12	9.73
Objective function	Basic, J	Min	0.0045	0.0061	0.0046	0.0026	**0.0021**
		Mean	0.0093	0.0096	0.0096	0.0048	0.0051
		Stdev	0.0018	0.0013	0.0019	0.0016	0.0013
	Swarming, J_{cc}	Min	−0.014	–	−0.015	−0.015	–
		Mean	−0.011	–	−0.011	−0.013	–
		Stdev	0.0032	–	0.0013	0.0012	–
	Overall, $J + J_{cc}$	Min	−0.009	–	−0.008	−0.012	–
		Mean	−0.002	–	−0.001	−0.008	–
		Stdev	0.0017	–	0.0019	0.002	–

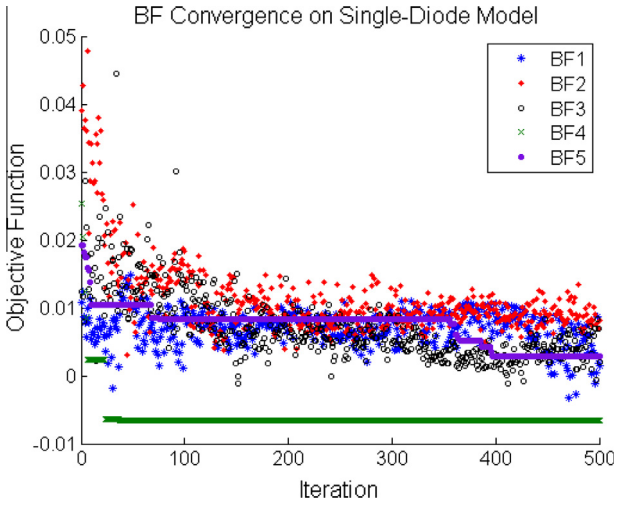

Fig. 5. Convergence behavior of BF variations on single-diode model.

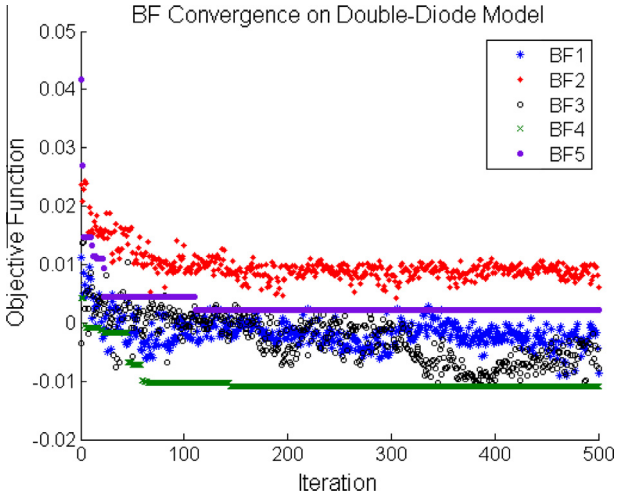

Fig. 6. Convergence behavior of BF variations on double-diode model.

versions, Table 3, and objective function cannot be negative, Figs. 5 and 6. The absolute best values of the basic objective function, *J*, are obtained using BF5; these values, shown in boldface in Table 3, are 0.0028 and 0.0021 for single- and double-diode models, respectively. Therefore, based on the optimization results, the most accurate sets of parameters of the present PV module are those obtained through BF5, which gave the least basic objective function, *J*, for both models.

One final comparison should be held between the results obtained using single-diode model and those of double-diode model. Using the same algorithm version, the double-diode model always yields lesser objective function values and requires longer time to converge. The lesser objective function values achieved through double-diode model are because of the higher accuracy by which this model represents the performance of the PV module. However, the longer convergence time is related to the more extensive mathematical computations required to solve the equivalent circuit as compared to the single-diode model.

5. Experimental verification

The output *I–V* characteristics of the Eclipsall NRG72 module are measured in the laboratory under different conditions. The test conditions vary in terms of the solar irradiance and temperature levels. In addition, some experiments are conducted under normal operation of uniform irradiance and temperature over all cells. Whereas, some other experiments are carried out under partial shading, where solar irradiance varies from one group of cells to the other. Partial shading conditions are created in reality by shadows of passing clouds, trees, towers, or nearby buildings when they cover part of the module. Usually, bypass and blocking diodes are used to prevent local hotspots in PV modules and arrays [45]. Bypass diodes protect series elements from accommodating high currents, and blocking diodes assures that currents of parallel strings are always feeding the load without feedback or circulation between strings. Out of the many tests performed on the Eclipsall module, selected cases are shown in Figs. 7 and 8 under different operating conditions. The mathematical model in [45] is used to compute the module performance under partial shading using (1)–(7).

Parameters obtained via BF5, as given in Table 3, are used to represent the PV module. Performance is computed using both the single- and double-diode models for the sake of comparison with experimentation. Fig. 7 shows measured and computed performance at two different normal operations. Partial shading comparison is depicted in Fig. 8 also at two different conditions. Experimental testing is carried out at high and low irradiance levels for both normal and partial shading operation. One of the partial shading cases of Fig. 8 reflects two different levels of irradiance on two groups of cells, while the other case on the same figure indicates three different levels on three groups of cells. On the low-irradiance curve of partial shading in Fig. 8, although the difference in irradiance between the first and second groups of cells is very small (129 W/m^2 and 115 W/m^2), the model parameters are still

Table 4
PV module parameters.

Parameter	BF1	BF2	BF3	BF4	BF5
Single-diode model					
R_s, Ohm	0.7139	0.742	0.7163	1.0432	0.9545
R_{sh}, Ohm	1412	1304	1260.1	1307.3	1427.4
k_i, %/°C	0.0643	0.0448	0.0022	0.08	0.0394
A_1	1.2014	1.1945	1.2091	1.0729	1.1111
I_{or1}, A	7.74×10^{-9}	6.69×10^{-9}	8.96×10^{-9}	6.67×10^{-10}	1.44×10^{-9}
Double-diode model					
R_s, Ohm	0.8875	0.7099	0.9463	1.0678	0.9932
R_{sh}, Ohm	1442.2	1402.5	1400.2	1309.4	1493.8
k_i, %/°C	0.0904	0.0511	0.0055	0.0482	0.0403
A_1	1.1282	1.1615	1.1124	1.0807	1.0914
I_{or1}, A	1.99×10^{-9}	3.58×10^{-9}	1.45×10^{-9}	7.61×10^{-10}	9.66×10^{-10}
A_2	1.592	1.501	1.5717	2.1189	1.7224
I_{or2}, A	2.77×10^{-10}	2.63×10^{-8}	5.83×10^{-10}	5.63×10^{-9}	1.67×10^{-8}

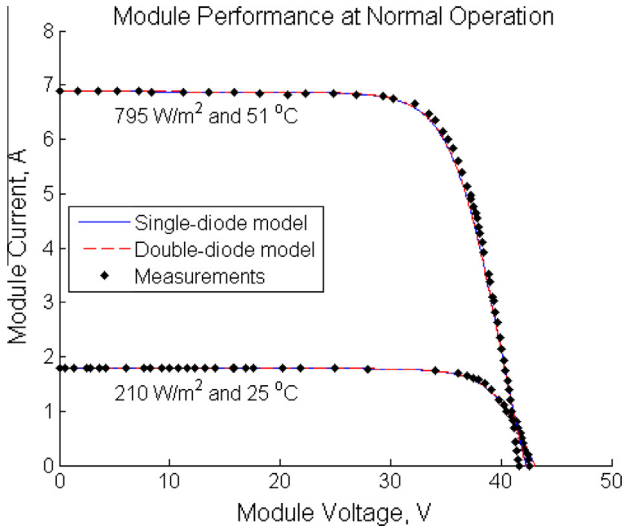

Fig. 7. Measured and computed performance of the Eclipsall PV module under different normal conditions.

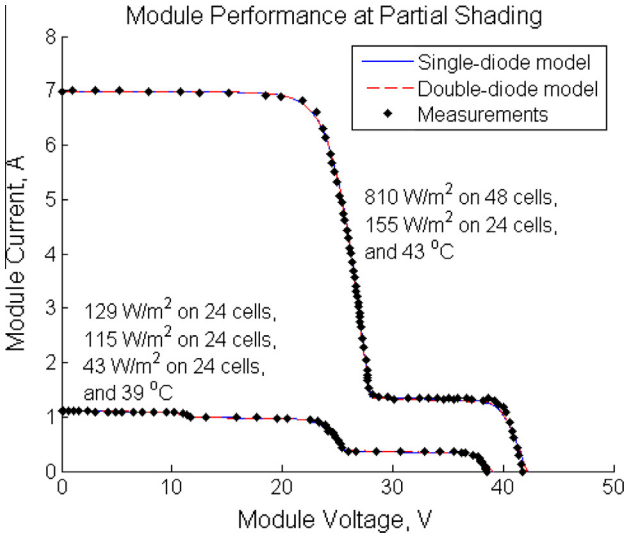

Fig. 8. Measured and computed performance of the Eclipsall PV module under different partial shading conditions.

accurately representing the module behavior. In general, the matching between measured and computed performance is acceptable despite the many random and systematic errors associated with experimental work in general. The matching is also sufficient to validate the research results. Finally, it should be noted from Figs. 7 and 8 that single- and double-diode models yield computed characteristic curves which are very close to each other. In other words, both models represent the PV module equally well on the ground of comparison with actual performance.

6. Conclusions

The paper presents a methodology to extract model parameters from the nameplate data of PV modules based on various versions of the BF optimization algorithm. An objective function expressing the discrepancy between targeted and computed performance is minimized. Targeted performance indices represent STC characteristics as given by the manufacturer via module nameplate. The technique is applied on both single- and double-diode PV models.

The original BF algorithm is varied by independently and concurrently ignoring swarming, varying the chemotactic step size, and preserving the global best function. Best solutions to the optimization problem are attained when all three variations are collectively implemented. Analysis of the results sheds some light on the impact of each individual variation on the behavior of BF algorithm.

Performance computed using parameters extracted by the most effective version of BF is compared to measurements under different operating conditions. Comparison of computation and experimentation is held at normal operation and partial shading under high and low solar irradiance. The acceptable matching between analytical and experimental characteristics shows the effectiveness of the proposed technique and validates the research results.

Distinct from available literature, the objective function formulation of this work is straightforward and avoids any mathematical derivation or approximating assumption. Moreover, the research explores, in different scenarios, possible enhancement of the behavior of BF algorithm as applied to the problem of PV parameter extraction. Some of the proposed modifications improve the optimization results when implemented individually. However, when all three modifications are collectively acting, optimization results are significantly enhanced. Therefore, findings of this research advise on the BF algorithm features which yield best results upon solving the problem of PV parameter identification. Finally, the BF variations presented in this paper could be particularly applied to parameter extraction of other electrical system elements, or broadly extended to different nonlinear multimodal optimization problems.

References

[1] Cubas J, Pindado S, Farrahi A. New method for analytical photovoltaic parameter extraction. In: Proc int conference on renewable energy research and applications, Madrid, Spain; 20–23 October, 2013. p. 873–7.
[2] Farivar G, Asaei B. A new approach for solar module temperature estimation using simple diode model. IEEE Trans Energy Convers 2011;26(4):1118–26.
[3] Chatterjee A, Keyhani A, Kapoor D. Identification of photovoltaic source models. IEEE Trans Energy Convers 2011;26(3):883–9.
[4] Lo Brano V, Orioli A, Ciulla G, Di Gangi A. An improved five-parameter model for photovoltaic modules. Sol Energy Mater Sol Cells 2010;94:1358–70.
[5] Silva E, Bradaschia F, Cavalcanti MC, Nascimento AJ. Parameter estimation method to improve the accuracy of photovoltaic electrical model. IEEE J Photovolt 2016;6(1):278–85.
[6] Chenni R, Makhlouf M, Kerbache T, Bouzid A. A detailed modeling method for photovoltaic cells. Energy 2007;32:1724–30.
[7] Lineykin S, Averbukh M, Kuperman A. An improved approach to extract the single-diode equivalent circuit parameters of a photovoltaic cell/panel. Renew Sustain Energy Rev 2014;30:282–9.
[8] Ortiz-Conde A, Sanchez FJG, Muci J. New method to extract the model parameters of solar cells from the explicit analytic solutions of their *I–V* characteristics. Sol Energy Mater Sol Cells 2006;90:352–61.
[9] Bouzidi K, Chegaar M, Bouhemadou A. Solar cells parameters evaluation considering the series and shunt resistance. Sol Energy Mater Sol Cells 2007;91:1647–51.
[10] de Blas MA, Torres JL, Prieto E, Garcia A. Selecting a suitable model for characterizing photovoltaic devices. Renewable Energy 2002;25:371–80.
[11] Chan DSH, Phillips JR, Phang JCH. A comparative study of extraction methods for solar cell model parameters. Solid-State Electron 1986;29(3):329–37.
[12] Ikegami T, Maezono T, Nakanishi F, Yamagata Y, Ebihara K. Estimation of equivalent circuit parameters of PV module and its application to optimal operation of PV system. Sol Energy Mater Sol Cells 2001;67:389–95.
[13] Haouari-Merbah M, Belhamel M, Tobias I, Ruiz JM. Extraction and analysis of solar cell parameters from the illuminated current-voltage curve. Sol Energy Mater Sol Cells 2005;87:225–33.
[14] Chegaar M, Azzouzi G, Mialhe P. Simple parameter extraction method for illuminated solar cells. Solid-State Electron. 2006;50:1234–7.
[15] Krishnakumar N, Venugopalan R, Rajasekar N. Bacterial foraging algorithm based parameter estimation of solar PV model. In: Proc int conference on microelectronics, communication, and renewable energy, Kanjirapally, Kerala, India; 4–6 June, 2013, p. 1–6.
[16] Ishaque K, Salam Z. An improved modeling method to determine the model parameters of photovoltaic (PV) modules using differential evolution (DE). Sol Energy 2011;85:2349–59.

[17] da Costa WT, Fardin JF, Simonetti DSL, Neto LVB. Identification of photovoltaic model parameters by differential evolution. In: Proc IEEE int conference on industrial technology, Vina del Mar, Chile; 14–17 March, 2010. p. 931–6.
[18] Ye M, Wang X, Xu Y. Parameter extraction of solar cells using particle swarm optimization. J Appl Phys 2009;105:094502.
[19] Sandrolini L, Artioli M, Reggiani U. Numerical method for the extraction of photovoltaic module double-diode model parameters through cluster analysis. Appl Energy 2010;87:442–51.
[20] Zagrouba M, Sellami A, Bouaicha M, Ksouri M. Identification of PV solar cells and modules parameters using the genetic algorithms: application to maximum power extraction. Sol Energy 2010;84:860–6.
[21] El-Naggar KM, Al-Rashidi MR, Al-Hajri MF, Al-Othman AK. Simulated annealing algorithm for photovoltaic parameters identification. Sol Energy 2012;86(1). pp.
[22] Attivissiomo F, Di Nisio A, Savino M. Uncertainty analysis in photovoltaic cell parameter estimation. IEEE Trans Instrum Meas 2012;61(5):1334–42.
[23] Barukcic M, Corluka V, Miklosevic K. The irradiance and temperature dependent mathematical model for estimation of photovoltaic panel performances. Energy Convers Manage 2015;101:229–38.
[24] Passino KM. Biomimicry of bacterial foraging for distributed optimization and control. IEEE Control Syst Mag 2002;22(3):52–67.
[25] Tang WJ, Li MS, Wu QH, Saunders JR. Bacterial foraging algorithm for optimal power flow in dynamic environments. IEEE Trans Circuits Syst I: Regul Papers 2008;55(8):2433–42.
[26] Okaeme NA, Zanchetta P. Hybrid bacterial foraging optimization strategy for automated experimental control design in electrical drives. IEEE Trans Ind Inform 2013;9(2):668–78.
[27] Eslamian M, Hosseinian SH, Vahidi B. Bacterial foraging-based solution to the unit-commitment problem. IEEE Trans Power Syst 2009;24(3):1478–88.
[28] Singh S, Ghose T, Goswami SK. Optimal feeder routing based on the bacterial foraging technique. IEEE Trans Power Delivery 2012;27(1):70–8.
[29] Nanda J, Mishra S, Saikai LC. Maiden application of bacterial foraging-based optimization technique in multiarea automatic generation control. IEEE Trans Power Syst 2009;24(2):602–9.
[30] Hooshmand RA, Soltani S. Fuzzy optimal phase balancing of radial and meshed distribution networks using BF-PSO algorithm. IEEE Trans Power Syst 2012;27 (1):47–57.
[31] Mishra S. A hybrid least square-fuzzy bacterial foraging strategy for harmonic estimation. IEEE Trans Evolut Comput 2005;9(1):61–73.
[32] Mishra S, Bhende CN. Bacterial foraging technique-based optimized active power filter for load compensation. IEEE Trans Power Delivery 2007;22 (1):457–65.
[33] Farahat IA, El-Hawary ME. Dynamic adaptive bacterial foraging algorithm for optimum economic dispatch with valve-point effects and wind power. IET Gener Transm Distrib 2010;4(9):989–99.
[34] Shao Y, Chen H. The optimization of cooperative bacterial foraging. In: Proc world congress on software engineering, Xiamen, China, vol. 2; 19–21 May, 2009. p. 519–23.
[35] Dasgupta S, Das S, Abraham A, Biswas A. Adaptive computational chemotaxis in bacterial foraging optimization: An analysis. IEEE Trans Evolut Comput 2009;13(4):919–41.
[36] Chen H, Zhu Y, Hu K. Self-adaptation in bacterial foraging optimization algorithm. In: Proc int conference on intelligent system and knowledge engineering, Xiamen, China; 17–19 November, 2008. p. 1026–31.
[37] Tang W, Wu Q, Saunders J. Bacterial foraging algorithm for dynamic environments. In: Proc IEEE congress on evolutionary computation, Vancouver, BC, Canada; 16–21 July, 2006. p. 1324–30.
[38] Panda R, Naik MK. A crossover bacterial foraging optimization algorithm. Appl Comput Intell Soft Comput 2012;2012 Article ID 907853.
[39] Munoz MA, Halgamuge SK, Alfonso W, Caicedo EF. Simplifying the bacteria foraging optimization algorithm. In: Proc ieee congress on evolutionary computation, Barcelona, Spain; 18–23 July, 2010. p. 1–7.
[40] Kim D, Abraham A, Cho JH. A hybrid genetic algorithm and bacterial foraging approach for global optimization. Inf Sci 2007;177:3918–37.
[41] Biswas A, Dasgupta S, Das S, Abraham A. A synergy of differential evolution and bacterial foraging optimization for global optimization. Neural Network World 2007;17(6):607–26.
[42] Biswas A, Dasgupta S, Das S, Abraham A. Synergy of PSO and bacterial foraging optimization – a comparative study on numerical benchmarks. Innovations Hybrid Intell Syst, 44. Springer; 2008. p. 255–63.
[43] Charles JP, Bordure G, Khoury A, Mialhe P. Consistency of the double exponential model with the physical mechanisms of conduction for a solar cell under illumination. J Phys – D: Appl Phys 1985;l8(11):2261–8.
[44] Das S, Dasgupta S, Biswas A, Abraham A, Konar A. On stability of the chemotactic dynamics in bacterial-foraging optimization algorithm. IEEE Trans Syst Man Cybern—Part A: Syst Humans 2009;39(3):670–9.
[45] Patel H, Agarwal V. Matlab-based modeling to study the effects of partial shading on PV array characteristics. IEEE Trans Energy Convers 2008;23 (1):302–10.